Assimilation of Radar Information in aLMo

Daniel Leuenberger and Andrea Rossa

MeteoSwiss, Krähbühlstrasse 58, 8044 Zürich, Switzerland

1 Introduction

Short-range and high-resolution numerical weather prediction (NWP) has a particular need for a proper definition of the initial model state. Especially when aiming at quantitative precipitation forecasting high-resolution observations of dynamical and thermodynamic quantities are required for the model initialisation to reduce the spin-up in the forecast. Since weather radars offer the possibility of retrieving high-resolution – both in time and space – observations of mesoscale precipitation related phenomena they become an increasingly important complement to conventional observations for assimilation into and verification of NWP models.

Various approaches to the assimilation of precipitation information have been developed over the last decade, including adjustment and nudging techniques as well as variational approaches (for a review see Alberoni et al., 2002). The COST-717 action 'On the Use of Radar Information in Hydrological and NWP Models' (Rossa, 2000) is the manifestation of the substantial interest in this field across Europe. On the other hand, the operational implementation has been realized only at a few weather services, and a best method has yet to emerge. NCEP uses an adjustment scheme to assimilate multi-sensor precipitation information (operational since July 2001, Lin, 2002) and since March 2002, the Japanese Meteorological Agency applies 4DVAR for the assimilation of radar derived precipitation (Koizumi et al., 2002).

We choose the Latent Heat Nudging (LHN) technique (e.g. Wang and Warner, 1988) because it is well in line with the nudging concept of the LM. Its main idea is to force the model with observed precipitation information during a pre-forecast period. An LHN algorithm, originally developed for satellite data by Manobianco et al. (1994) was adopted for the assimilation of radar-derived surface precipitation by Jones and Macpherson (1997) and has been successfully run in operational mode at the UK Metoffice (Macpherson, 2001).

In this contribution we report on the current development state of the LHN at MeteoSwiss and present preliminary results of a case study with the Alpine Model (aLMo), the Swiss version of the LM.

2 Radar Data

Estimating surface rain rates from radar observations, especially in complex terrain, is a challenging task. Since radar is a remote sensing system and measures only backscattered electromagnetic signals, the derivation of quantitative rain rates at the ground suffers from a number of problems, notably: ground clutter, partial beam blocking resulting in areas with low visibility, bright band effects, anomalous propagation, beam attenuation (especially for long ranges and cases of intense precipitation) and side lobe or second trip echoes. However, effort has been put into overcoming some of the above mentioned problems in the past years

and they continue to be tackled. Nevertheless, radar measurements provide high quality rain/no rain information within the range of the radar site at a high spatial and temporal resolution.

The Swiss Radar Network (SRN, Joss et al., 1998) consists of three C-band Doppler Radars of the same type, providing full volume information every five minutes. The data are pre-processed and available on a cartesian grid with a mesh size of $1 \times 1 \times 1\,km^3$ for single radar sites and $2 \times 2 \times 2\,km^3$ for the network composite. In this study we use the best estimate of surface precipitation where many state of the art corrections have been applied to, including clutter elimination and vertical profile correction algorithms. The precipitation rates are averaged over the last 6 samples (30 min) to improve the representativity and robustness to data losses and are interpolated onto the model grid.

3 The LHN Method

The main principle of the LHN is to correct the model's latent heating (LH) at each time step by an amount derived from observed and model estimated precipitation. One of the major challenges is the determination of the LH. A common approach is to relate the vertically integrated heating in an atmospheric column to the surface precipitation rate. This is based on the observation that relatively little moisture is stored in clouds. The horizontal distribution of observed surface precipitation gives information about the location and the approximate amount of the released/absorbed LH. However, the vertical distribution of the heating is not known. Manobianco et al. (1994) and Jones and Macpherson (1997) used model profiles to deduce the vertical partitioning, based on the assumption, that they have a realistic vertical shape. The basic concept of the LHN in LM is as follows:

- First, the model physics and the dynamic tendencies are derived from the current state of the model atmosphere.
- Then the diabatic temperature tendencies related to phase changes of water for each grid point are calculated (hereafter related to as model latent heating (LH)).
- Finally, the LHN temperature increments for each grid point are calculated by scaling the profile with a factor determined from the radar-derived and the model surface rain rate and are added to the prognostic temperature field at the end of the time step.

These steps are described in more detail in the following subsections.

3.1 Calculation of the model Latent Heating

Contributions to the source/sink of LH are dependent on the precipitation parametrisation scheme in use. For this study we use the one-category ice scheme described in section 7.4 of the LM scientific documentation (Doms and Schättler (1999). In this case, the discrete LH is calculated from

$$LH = \frac{\Delta T_{LH_{mod}}}{\Delta t} = \frac{L_V}{c_{pd}}\left(S_c - S_{ev}\right) + \frac{L_S}{c_{pd}}\,S_{dep} + \frac{L_F}{c_{pd}}\left(S_{nuc} + S_{rim} + S_{frz} - S_{melt}\right) \qquad (1)$$

where L_V and L_S are, respectively, the latent heat of vapourization and of sublimation and $L_F = L_S - L_V$ is the latent heat of fusion. c_{pd} denotes the specific heat of dry air at constant pressure, Δt is the model time step. The mass transfer rates S_x are listed in Table 1.

Symbol	Definition / Description
S_c	Condensation and evaporation of cloud water.
S_{ev}	Evaporation of rain in sub-cloud layers.
S_{dep}	Depositional growth of snow.
S_{nuc}	Initial formation of snow due to nucleation from cloud water.
S_{rim}	Accretion of cloud water by snow (riming), $T < 273.16K$.
S_{frz}	Heterogeneous freezing of rain to from snow, $T < 267.16K$.
S_{melt}	Melting of snow to form rain, $T > 273.16K$.

Table 1: Mass transfer rates contributing to the release/absorption of latent heat

If the new two-category ice scheme (see Doms and Schättler, 1999, section 7.5) is applied, additional source/sink terms S_x must be considered. If the convection parametrisation is switched on, an extra convective temperature tendency is added to LH.

3.2 Calculation of the LHN Temperature increments

The LHN Temperature increments ΔT_{LHN} added to the prognostic temperature field at the end of the time step are now determined from model latent heat tendencies LH, the radar-estimated surface precipitation rate RR_{rad} and the model surface precipitation rate RR_{mod} from

$$\Delta T_{LHN} = (f-1) \cdot \Delta T_{LH_{mod}} \,, \quad f = RR_{ana}/RR_{mod} \tag{2}$$

where f is the scaling factor determined from the ratio of the analysed and the model rain rate. The analysed rain rate RR_{ana} is a weighted sum of the radar-estimated and the model rain rate:

$$RR_{ana} = w \cdot RR_{rad} + (1-w) \cdot RR_{mod}. \tag{3}$$

We have introduced the observation weight $w = w(x,y,t), w \in [0,1]$ which serves as a quality information for the radar-estimated rain rate. It takes high values for regions with a good radar coverage and low values for regions with poor coverage. For $w = 1$ the analysed rain rate is equal to the radar-estimated rain rate, $w = 0$ does not consider radar information and the analysed rain rate equals the model rain rate. Jones and Macpherson (1997) propose to

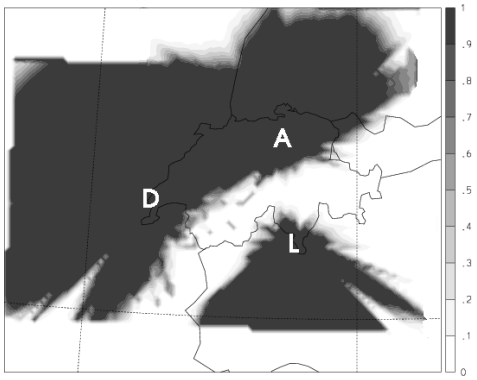

Figure 1: Spatial distribution of the observation weight w for the domain covered by the Swiss Radar Network. The letters indicate the respective position of the three radar sites Dole, Albis and Lema. The dark areas mark regions with good radar coverage, white areas mark region with poor or no coverage.

use the distance to the nearest radar site as measure for the radar quality with high quality near a radar site and low quality more distant of it. In regions with complex terrain, where radar measurements are hampered by partial beam blocking or ground clutter, we consider it as more appropriate to use the height above sea level of the lowest unblocked radar beam from the nearest radar site as quality information. This minimal height is then mapped to the interval [0,1] where w is equal to unity for a height less than $2000\,m$ and decreases gradually to zero at a height of $4000\,m$. Figure 1 shows the spatial distribution of w for the three radar sites of the Swiss Radar Network.

If there are large discrepancies between observed and modelled rain rates, the scaling factor f is limited so that there is not too much heat added to or removed from the model. If at a grid point the observed rain rate is much larger than the model rain rate (this includes the case, where the model has no precipitation) no suitable profile is provided by the model and a nearby grid point is searched within a given range, where the rain rate more closely matches the local observed rain rate. If such a point is found, the nearby profile is scaled. If no nearby point is found, an idealised Latent Heat profile is used for the scaling. In Table 2 the possible ranges for the ratio between observed and model rain rates and the corresponding scaling factor and profile are listed.

		scaling factor f	profile to scale
model fair:	$1/\alpha_{down} \leq \frac{RR_{ana}}{RR_{mod}} \leq \alpha_{up}$	$\frac{RR_{ana}}{RR_{mod}}$	local profile
model too wet:	$\frac{RR_{ana}}{RR_{mod}} \leq 1/\alpha_{down}$	$1/\alpha_{down}$	local profile
model too dry:	$\frac{RR_{ana}}{RR_{mod}} \geq \alpha_{up}$	$\frac{RR_{ana}}{RR_{near/ideal}}$	nearby/ideal. profile

Table 2: Ratios of observed and model rain rates and corresponding scaling factors and profiles. We use values of $\alpha_{down} = \alpha_{up} = 3$ as proposed by Jones and Macpherson (1997).

4 Case study

The current version of the LHN scheme in the aLMo has been tested on a case study of severe convection over the Swiss Plateau. This particular system has been selected because of its coherent structure and its long retention period in the SRN domain. First we briefly describe the meteorological situation and then present results of aLMo analyses and forecasts.

4.1 Overview of the Meteorological Situation

On 20 August 2000 a system of deep convection formed ahead of a cold front over central France which has associated a well developed, elongated, quasi-stationary upper-level trough featuring wind speeds of up to 50 knots on the $500\,hPa$ analysis (not shown). The convection was orographically triggered around 22:30 UTC over the French Massif Central, developed in a distinct band of strong southwesterly wind (Figure 2a) and continued its way across the Swiss Plateau, where it gained strength before decaying in southern Germany. At its stage of maximum intensity the system was accompanied by violent wind gusts causing severe

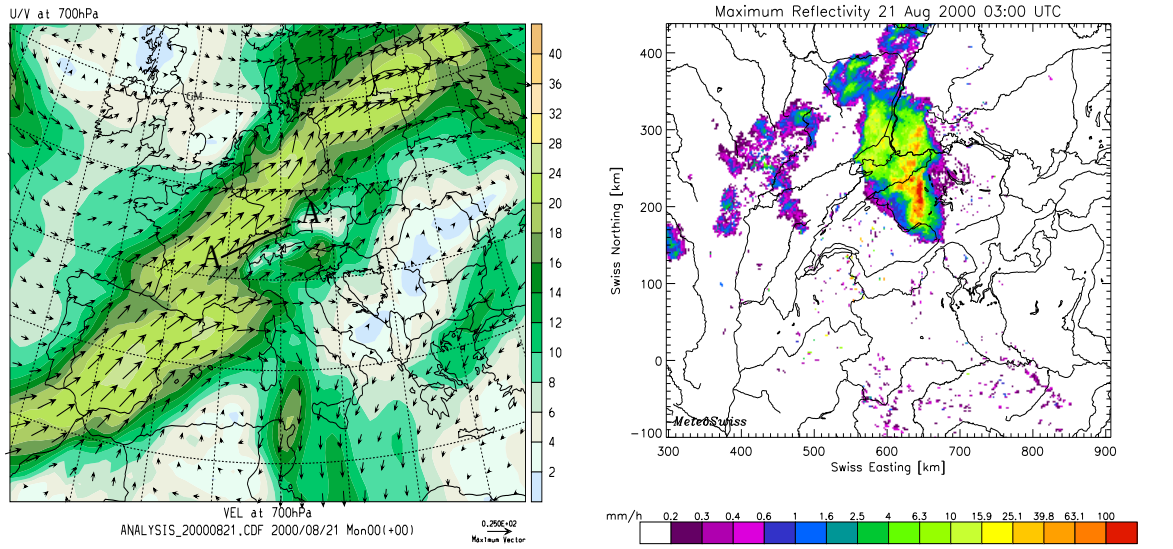

a) b)

Figure 2: a) ECMWF analysis of 700 hPa wind $[m/s]$ at 21 August 2000, 00 UTC and b) Swiss radar composite of maximum reflectivity at 21 August 2000, 03 UTC

damage in eastern Switzerland. Figure 2b shows a SRN composite image of maximum radar reflectivity at 03 UTC. Red areas mark regions with reflectivities above 55 dBZ or 100 mm/h, illustrating the magnitude of the event.

4.2 aLMo Analysis

Several aLMo simulation of this case have been carried out. The model is run on the operational domain of MeteoSwiss using a horizontal mesh width of 7 km. For all simulations the convective parametrisation scheme is switched on. The control forecast (CTRL) of 21 August 00 UTC is started from and laterally driven by GME. An LHN analysis (LHN_ANA) is performed with the continuous assimilation of radar data from 00 to 06 UTC. Figure 3 shows modeled and observed (right panels) precipitation sums over the SRN domain. The CTRL simulation (left panels) completely misses the convective event since the initial condition does not contain the small-scale information needed to trigger convection. A misplaced stratiform rain band (not observed by radar) is visible in the western part of the SRN domain.

The LHN simulation (central panels) produces a rainfall pattern well in agreement with the observed one. Moreover the LHN scheme is able to correct to some extent the misplaced frontal precipitation structure apparent in the CTRL run. In Figure 4 we document the feedback of the LHN scheme to the model dynamics. A vertical cross-section of relative humidity, potential temperature and vertical velocity (panel a) along the storm track (line from A to A' in Figure 2) evidences the LHN-induced deep circulation featuring a tower of saturated air up to the tropopause, strong temperature gradients in the outflow region of the storm and distinct areas of intense updraft of several m/s. Panel b shows the 10 m windspeed at 04 UTC over Switzerland. To compare the aLMo field with observations, the 10 m windspeed measured by a number of mesonet stations at the same time is plotted as coloured dots. Only stations north of the Alps and situated below 800m ASL are shown. A coherent area of strong winds is evident in the model field. Most of the stations near this region also measure enhanced winds. Shown are wind speeds averaged over 10 minutes. Maximum gusts during this period, however, exceed these means by a factor of 2 to 3 (not shown).

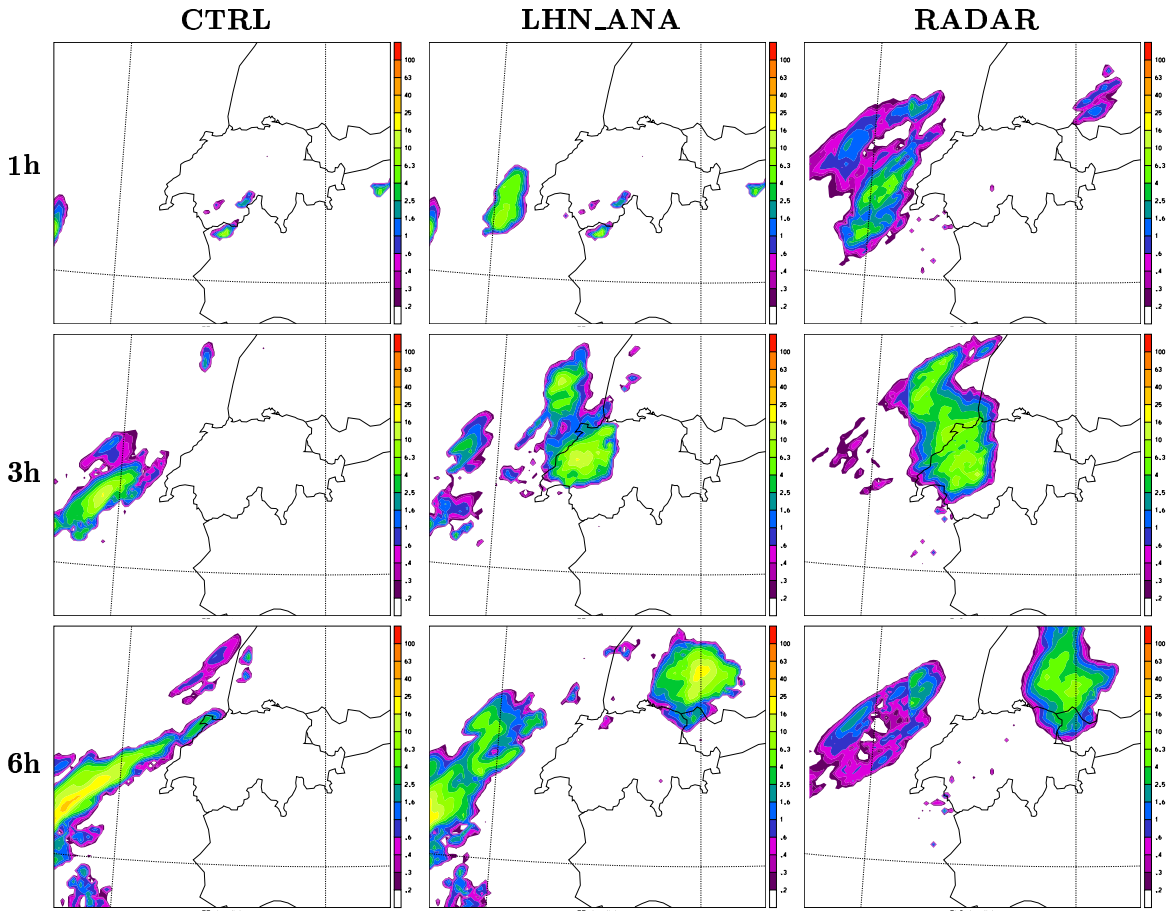

Figure 3: Hourly sums of radar-observed and modeled precipitation $[mm/h]$. Left panels show aLMo control simulations, central panels aLMo LHN-analyses and right panels radar observations. First row depict sums from 00-01 UTC, second row from 02-03 UTC and third row from 05-06 UTC.

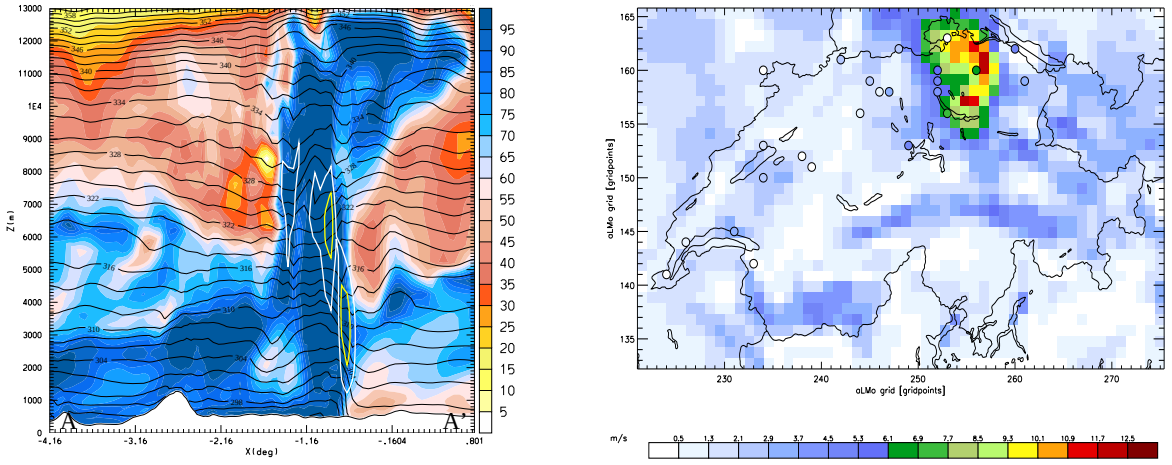

a) RH, θ and W at 04 UTC

b) 10m wind at 04 UTC

Figure 4: Dynamical fields of the LHN analysis at 04 UTC. a) Vertical cross-section of relative humidity [%], potential temperature $[K]$ and vertical velocity $[m/s]$, white contour for $1\,m/s$ and yellow contour for $2\,m/s$, b) $10\,m$-windspeed $[m/s]$. Coloured dots represent observed windspeeds from automatic mesonet stations of MeteoSwiss at the same time

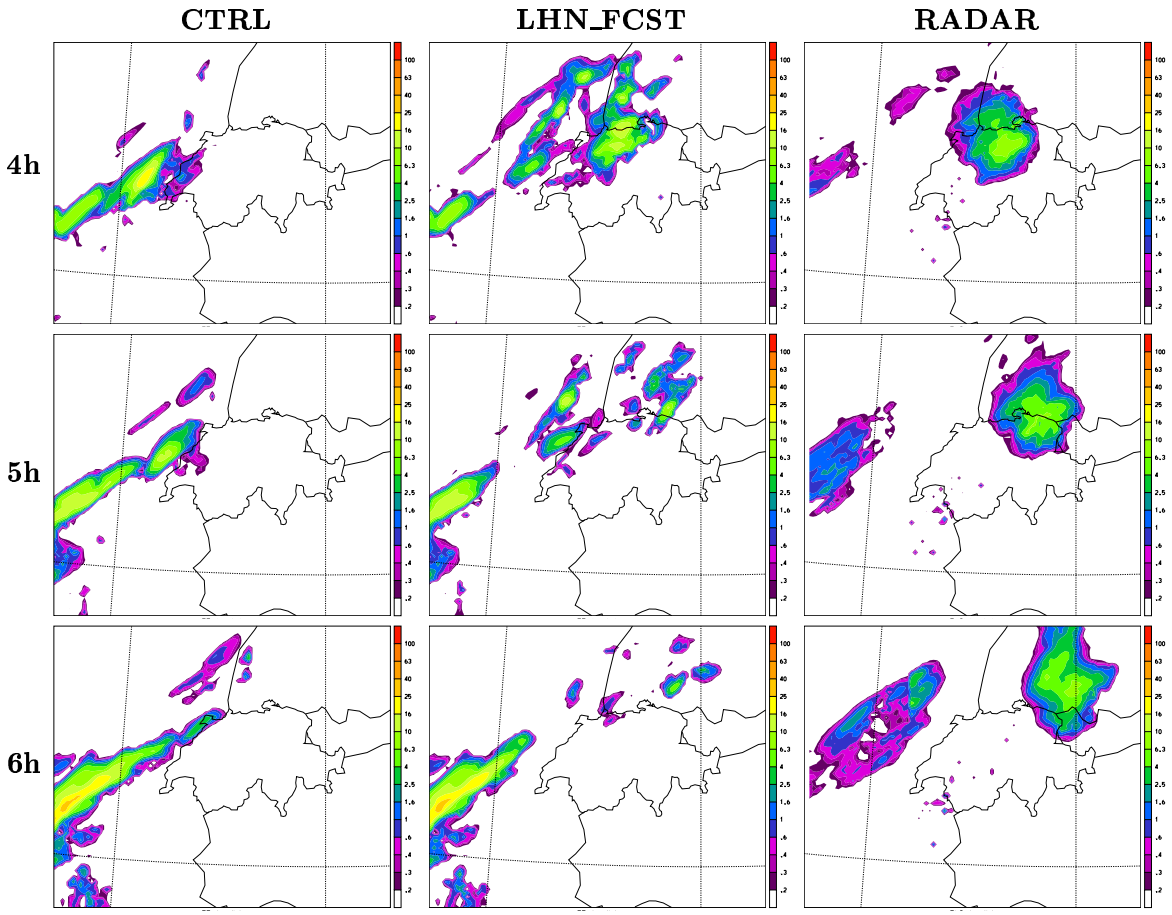

Figure 5: Hourly sums of radar-observed and modeled precipitation $[mm/h]$. Left panels show aLMo control simulations, central panels LHN-forecasts and right panels radar observations.

4.3 aLMo Forecast

In a second simulation we only assimilate radar data during the first three hours and continue in forecast mode for another three hours. Figure 5 shows hourly sums of modeled and observed precipitation from 03 UTC to 06 UTC, i.e. after the LHN scheme has been switched off. The precipitation produced by the LHN-forecast (central panels) is still in reasonable agreement after one hour free forecast (first row). However, the further evolution of the storm is not well captured by the model and the assimilated radar information vanishes during the two following forecast hours (second and third row). In addition the frontal precipitation in the western part of the SRN domain is no longer corrected and regains strength after the LHN forcing has stopped.

5 Summary and Outlook

We have tested the LHN algorithm in aLMo using surface precipitation derived from SRN measurements on a severe convection case.

- Overall, the scheme is able to trigger a convective system with associated precipitation patterns in good agreement, both in position and amplitude, with those observed by radar.

- Moreover, the dynamical response features the formation of a realistic, deep circulation associated with surface winds which correspond well with mesonet observations.

This demonstrates the value of the mesoscale analysis using only temperature increments derived from radar observations. However, despite the well developed circulation at the beginning of the free forecast, the model is not able to keep the assimilated information resulting in a premature decay of the storm. This could be due to a improper model representation of the meteorological environment in which the storm develops. As next steps we plan to

- use aLMo analyses using conventional data instead of interpolated GME fields for the initial and boundary conditions of the LHN runs. This may beneficially influence the quality of the LHN analysis and forecast.
- study the sensitivity of the vertical structure of assimilated latent heating by means of idealised observing system simulation experiments (OSSE) of a convective system and real case studies.

The investigation of this sensitivity is considered as the next step towards the further development of the LHN, particularly with regard to the addition of more radar information in order to determine the vertical latent heat distribution based on observations instead of the model.

Acknowledgements

We would like to express our gratitude to Dr. C. Koepken (ECMWF) for providing us with a LHN code for an early version of the LM and to Dr. G. Haase (SMHI) for inducting us into this code.

References

Alberoni, P.P., V. Ducrocq, G. Gregoric, G. Haase, I. Hollemann, M. Lindskog, B. Macpherson, M. Nuret, and A. Rossa, 2001: Quality and Assimilation of Radar Data for NWP – a Review, available from *http://www.smhi.se/cost717/*

Doms, G. and U.Schättler, 1999: The Nonhydrostatic Limited-Area Model LM (Lokal-Modell) of DWD: Part I, Scientific Documentation, available from
http://www.cosmo-model.org/

Jones, C. D. and B. Macpherson, 1997: A Latent Heat Nudging Scheme for the Assimilation of Precipitation Data into an Operational Mesoscale Model. *Meteorol. Appl.*, **4**, 269-277

Joss, J., B. Schädler, G. Galli, R. Cavalli, M. Boscacci, E. Held, G. della Bruna, G. Kappenberger, V. Nespor and R. Spiess, 1998: Operational Use of Radar for Precipitation Measurements in Switzerland. *Final Report of NRP31* ,vdf Hochschulverlag an der ETH Zürich, 108 pp., ISBN 3 7281 2501 6, http://vdf.ethz.ch

Macpherson, B., 2001: Operational Experience with Assimilation of Rainfall Data in the Met Office Mesoscale Model. *Meteorol. Atmos. Phys.*, **76**, 3-8

Koizumi, K., Y. Ishikawa, T. Tsuyuki and S. Murakami, 2002: Improvement in Precipitation Forecasts of the JMA Mesoscale Model with Four-Dimensional Variational Data Assimilation, available from
http://member.nifty.ne.jp/PennaeAquilae/Documents/QPF_92.ppt

Lin, Y., 2002, Test Assimilations of the Real Time, Multi-Sensor hourly Precipitation Analysis into the NCEP ETA Model, available from
http://www.emc.ncep.noaa.gov/mmb/papers/lin/pcpasm/paper.html

Manobianco, J., S. Koch, V. M. Karyampudi, and A. J. Negri, 1994: The Impact of Assimilating Satellite-Derived Precipitation Rates on Numerical Simulations of the ERICA IOP4 Cyclone. *Monthly Weather Review*, **122**, 341-365

Rossa, A. M., 2000: COST-717: Use of Radar Observations in Hydrological and NWP Models. *Phys. Chem. Earth (B)*, **25**, 1221-1224

Wang, W. and T. T. Warner, 1988: Use of Four-Dimensional Data Assimilation by Newtonian Relaxation and Latent-Heat Forcing to Improve a Mesoscale-Model Precipitation Forecast: A Case Study. *Monthly Weather Review*, **116**, 2593-2613